



Optics Letters

Probing electron–atom collision dynamics in gas plasma by high-order harmonic spectroscopy

PENGFEE WEI,^{1,2,†} MEIYAN QIN,^{3,4,†} XIAOLONG YUAN,^{2,†} CANDONG LIU,^{2,†} RUXIN LI,^{2,7} ZHINAN ZENG,² PEIXIANG LU,^{3,8} KONSTANTIN DORFMAN,^{5,6,9} WEIGUO YE,¹ BO YAO,¹ QI JIE WANG,⁴ HAO LI,⁶ JIAYUN LIU,⁶ YING ZHANG,⁶ SEOK YONG JEONG,⁷ GUNSU S. YUN,⁷ AND DONG EON KIM^{7,10}

¹Department of Physics, Shaoxing University, Shaoxing 312000, China

²State Key Laboratory of High Field Laser Physics, Shanghai Institute of Optics and Fine Mechanics, CAS, Shanghai 201800, China

³Laboratory of Optical Information Technology, Wuhan Institute of Technology, Wuhan 430205, China

⁴School of Electrical and Electronic Engineering, Nanyang Technological University, Nanyang Avenue 639798, Singapore

⁵State Key Laboratory of Precision Spectroscopy, East China Normal University, Shanghai 200062, China

⁶Singapore Institute of Manufacturing Technology, Innovis 138634, Singapore

⁷Physics Department and Center for Attosecond Science and Technology, POSTECH and Max Planck POSTECH/KOREA Research Initiative, Pohang 37673, South Korea

⁸e-mail: lupeixiang@hust.edu.cn

⁹e-mail: dorfman@ps.ecnu.edu.cn

¹⁰e-mail: kimd@postech.ac.kr

[†]e-mail: ruxinli@shcnc.ac.cn

Received 20 February 2018; revised 21 March 2018; accepted 21 March 2018; posted 23 March 2018 (Doc. ID 324509); published 17 April 2018

Plasma is a complex system involving diverse collisional processes and interactions, such as electron-impact excitation, ionization, recombination, etc. One of the most important methods for studying the properties and dynamics of plasma is to analyze the radiations from plasma. Here, we demonstrate the high-order harmonic (HH) spectroscopy for probing the complex electron–atom collision (EAC) dynamics in a laser-induced gas plasma. These measurements were carried out by using an elliptically polarized pump and a time-delayed linearly polarized probe. The HH spectra from argon and krypton plasmas were recorded by scanning the time delay up to hundreds of picoseconds. We found that the delay-dependent HH yield contains three distinct regions, i.e., the first enhancement, the subsequent suppression, and the final restoration regions. A qualitative analysis shows that these features are clear signatures of the EAC processes and interactions involved in the delay-dependent HH spectroscopy. © 2018 Optical Society of America

OCIS codes: (020.2649) Strong field laser physics; (190.2620) Harmonic generation and mixing; (320.2250) Femtosecond phenomena; (320.7110) Ultrafast nonlinear optics.

<https://doi.org/10.1364/OL.43.001970>

Plasma [1–3] is one of the four fundamental states of matter consisting of hot electrons, ions in ground or excited states, and neutral atoms in ground or excited states. Unlike the other three states of matter (i.e., gas, liquid, and solid), plasma rarely exists on Earth under normal surface conditions, but can be usually laser-induced from neutral gas and will spontaneously

evolve into neutral gas after being generated [4,5]. For example, Mitryukovskiy *et al.* [5] investigated plasma luminescence from femtosecond filaments in the air and presented the evidence for impact excitation with circularly polarized light pulses. During this process, various dynamics can occur, among which electron–atom collision (EAC) is one of the most fundamental processes. The EAC can lead to the electron-impact excitation [6–8] or the electron-impact ionization [9–11]. Moreover, it has been demonstrated that the excited/ionized medium can enhance/suppress the high-order harmonic (HH) generation [12–15]. These characteristics provide a novel method for revealing the EAC dynamics through the observation of the HH signal. The deep understanding of EAC dynamics in plasma can not only provide an insight into the complicated evolution of plasma, but also help to find the optimum conditions for efficient HH generation from plasma. Recently, HH spectroscopy has been widely used in the study of ultrafast electron dynamics in atoms [13,16], chemical reaction and electron dynamics in molecules [17–20], and electron dynamics in solids [21]. Further extension of the HH spectroscopy to the plasma dynamics is a valuable contribution to the field of ultrafast measurement, which has been rarely reported so far.

In this Letter, an elliptically polarized laser is introduced as a pump pulse to produce a gas plasma, while a linearly polarized laser is employed as a probe pulse to drive the HH emission. The HH spectra as a function of the inter pulse time delay up to hundreds of picoseconds reveal three distinct regions consisting of the first enhancement region, the subsequent suppression region, and the final restoration region, which are closely related to and well explained by the electron-impact excitation, ionization, and recombination. Moreover, we found a quantitative difference between the delay-dependent HH spectra

from argon and krypton, which can be attributed to their different collision cross sections. Our experiment successfully extends the application of HH spectroscopy to the plasma phase, and demonstrates that the HH spectroscopy is a useful tool to probe the EAC process in plasma.

In our experiment (the output beam of a laser system, 8 mJ/45 fs/1 kHz at 800 nm, is split into two beams for this pump-probe scheme; after a time-delay setup, the two beams are focused by convex lenses with a focal length of 500 mm on the center of a 25-mm long gas cell located in a high-vacuum interaction chamber; more details are presented in Ref. [12]), to ensure that the collected HHs are primarily generated by the linearly polarized probe pulse, an ellipticity of 0.35 is introduced into the pump pulse to suppress the HH generation by the pump pulse itself [22]. According to the Ammosov–Delone–Krainov (ADK) theory [23], the population of species in the gas plasma generated by the pump laser pulse depends on the pulse intensity. Hence, the HH signal from the gas plasma also depends on the pump laser intensity. Accordingly, we carried out a series of experiments for different intensities of the pump laser. The pump laser intensity is varied from 0 W/cm² to 5×10^{14} W/cm², while the probe intensity is kept constant to be about 2×10^{14} W/cm². At this proper intensity of the probe pulse, only neutral atoms in the ground or excited states generate the HH signal, while no significant HH signals are generated from the ionized atoms. The delay of the probe pulse with respect to the pump is fixed at 3 ps. At this large delay, the pump pulse does not overlap with the probe pulse in time. This ensures that the gas plasma is generated only by the interaction with the pump pulse, and the HHs are emitted by the gas plasma interacting with the probe pulse. Gas pressure for both argon and krypton is chosen at 20 Torr in order to obtain the optimal HH signal.

In Figs. 1(a) and 1(b), the measured HH spectra for pump laser pulses of various intensities are presented for argon and krypton gas plasma, respectively. One can notice three distinct features in the spectra for both argon and krypton, i.e., normal HH signals at a low pump intensity, enhanced HH signals at a moderate pump intensity, and suppressed HH signals at a high pump intensity. To analyze the behavior of the HHs, the integrated signals over the whole spectra (dotted black line), along with the populations of neutral (solid black line), singly ionized ion (dashed green line), and doubly ionized ion (dotted red line), are presented as a function of the pump laser intensities in Figs. 2(a) and 2(b) for argon and krypton, respectively. The ionization rates of argon and krypton by the pump laser are calculated based on the ADK theory [23]. As depicted by the dotted black lines in Figs. 2(a) and 2(b), the integrated HH signals of argon and krypton show the same behavior

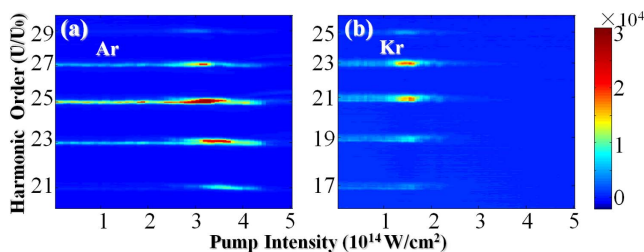


Fig. 1. HH signals measured as a function of pump intensity at a time delay of about 3 ps for argon (a) and krypton (b).

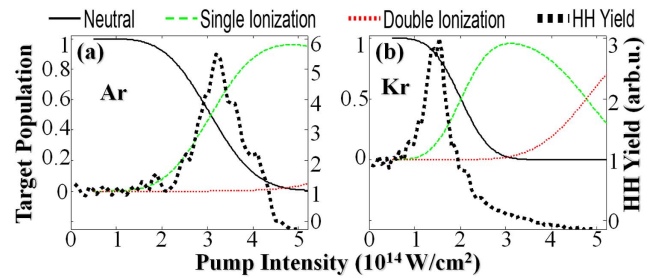


Fig. 2. Calculated population (left axis) of neutrals (black line), singly ionized atoms (dashed green line), and doubly ionized atoms (dotted red line) as a function of pump intensity for argon (a) and krypton (b), together with the HH yield (dotted black line for right axis) obtained by summing over all the HHs shown in Fig. 1.

as a single harmonic. For the case of argon shown in Fig. 2(a), the normal signal is observed when the pump intensity is lower than 2.0×10^{14} W/cm². For this range of intensity, the species in the gas plasma generated by the pump laser are dominated by the neutral argon, as shown by the solid black line. When the pump laser intensity increases above 2.0×10^{14} W/cm², but is lower than 4.3×10^{14} W/cm², the HH signal is enhanced. For this range of moderate intensity, neutral argon, hot electron, and singly ionized argon are dominant in the gas plasma. Since the intensity of the probe laser is controlled to produce HH from the neutral atoms in ground or excited states only, the enhanced signal may come from the excited states [12–15] or coherent superposition of states [24–27], which can be generated by the EAC [6–8]. When the pump intensity is higher than 4.3×10^{14} W/cm², the gas plasma mainly consists of hot electron and singly ionized argon, as shown by the solid black line and the dashed green line in Fig. 2(a). Consequently, HH emission is greatly suppressed, as shown by the dotted black line in Fig. 2(a). As for the case of krypton, the normal HH signal is observed below the intensity of 0.9×10^{14} W/cm², and the enhanced HH signal occurs for the pump intensity ranging from 0.9×10^{14} W/cm² to 1.9×10^{14} W/cm², which is followed by an obvious suppression of HH generation. Similar to the case of argon, the normal, enhanced, and suppressed HH signals are associated with the ground state, the excitation state, and the ionization state of krypton, respectively, as demonstrated by the solid black line and the dashed green line in Fig. 2(b). The major differences between argon and krypton are the location and extent of the enhancement. These may be due to the lower ionization energy and the larger cross section of krypton. For a target with a lower ionization energy, the intensity of the pump pulse required to generate gas plasma is lower. Meanwhile, the excited state of a target generated by the electron-impact excitation is easier to be destroyed by the electron-impact ionization, if the target has a larger cross section. Hence, the enhancement of the HH signal decays very quickly in the case of krypton, which leads to a narrow region for the harmonic enhancement. From Figs. 2(a) and 2(b), one can see that the maximum enhancement is observed at the pump intensity of 3.1×10^{14} W/cm² for argon and 1.5×10^{14} W/cm² for krypton. For these optimal intensities of pump pulse, the effect of the excited state generated by EAC is the strongest. Hence, we choose these pump intensities to investigate the EAC dynamics occurring in the argon and krypton gas plasma.

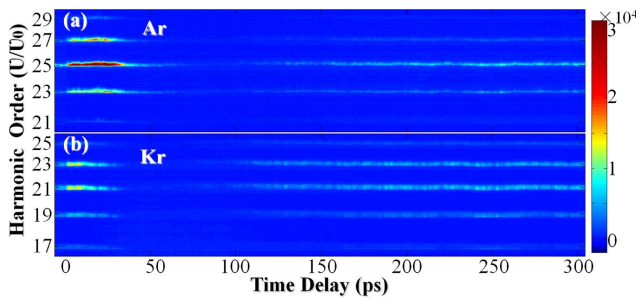


Fig. 3. HH signals measured for argon (a) and krypton (b) as a function of delay between the pump and probe pulses.

Using the optimal pump intensities discussed above, we have recorded HH signals as a function of time delay between the pump and probe pulses up to hundreds of picoseconds. The delay dependences of the HH signal from the argon and krypton plasma are shown in Figs. 3(a) and 3(b), respectively. Their corresponding integrations over all the HHs are shown in Fig. 4(a) by the black triangles and the blue circles, respectively. For the two targets, both the single [Figs. 3(a) and 3(b)] and the integrated [Fig. 4(a)] HH signals present three distinct regions, i.e., the enhancement, the suppression, and the restoration regions. As shown by the integrated HH signals in Fig. 4(a), there exist four important delay timescales in the delay-dependent HH signal. The first one corresponds to the significant enhancement of the HHs, i.e., the rise time of the HH enhancement. For the case of argon, it occurs around 5.5 ps, while for the case of krypton, it occurs around 3 ps. The second one represents the moment when the enhancement of the HHs starts to decay. It occurs around 25 ps for argon and 20 ps for krypton. The third corresponds to the beginning of the revival process for the HHs. It occurs around 100 ps for argon and 60 ps for krypton. The fourth one shows up when the HH signals fully revive. It occurs around 400 ps for argon and 200 ps for krypton.

For the sake of simplicity, atoms are considered stationary because they are much heavier than electrons. To show that these four important delays are closely related to the EAC dynamics, the mean collision time between electrons and atoms is estimated by

$$t_{e\text{-atom}} = \frac{\lambda_{e\text{-atom}}}{v_e} = \frac{(n\sigma)^{-1}}{(2E_k/m_e)^{1/2}} = \frac{k_B T m_e^{1/2}}{\sqrt{2}\eta P \sigma E_k^{1/2}}, \quad (1)$$

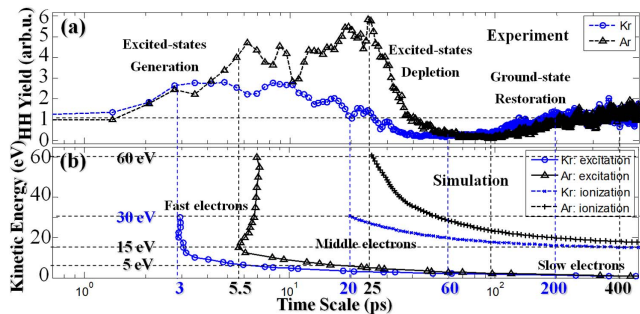


Fig. 4. (a) HH yield obtained by summing over all the HHs shown in Fig. 3. (b) Mean collision time for the collision excitation and ionization between electrons and atoms as a function of electron kinetic energy. The time delay is in logarithmic coordinate.

where $v_e = \sqrt{\frac{2E_k}{m_e}}$ is the velocity of the free electron, E_k is the kinetic energy of the free electron, m_e is the mass of electron, $n = \frac{\eta P}{k_B T}$ is the number density of the target atoms, k_B is the Boltzmann constant, T is the atom temperature ($T = 300$ K), η is the population of the target atom, P is the gas pressure, and σ is the cross section obtained from the experimental data [28–30]. In our simulation, the total cross section σ , which is related to all the interactions, is used to predict the first collisional time corresponding to the rise time of harmonic enhancement; the ionization cross section σ is also used to reveal the depletion time. At an experimental pump intensity of 3.1×10^{14} W/cm² for argon and 1.5×10^{14} W/cm² for krypton, the populations η of the remaining neutrals can be estimated to be about 50% for argon and 85% for krypton by ADK theory [23].

Using the experimental results, the maximum kinetic energies E_k of the free electrons are estimated to be about 60 eV for argon and 30 eV for krypton, i.e., 3.24 Up for argon and 3.35 Up for krypton, where Up is the ponderomotive energy. Since the value of σ varies with kinetic energy E_k of the impact electron [28–30], mean collision time between electrons and atoms for the above situations is presented as a function of electron kinetic energy, as shown in Fig. 4(b). The black triangles and the blue circles correspond to the mean collision time for the electron-impact excitation of argon and krypton, respectively. The black crosses and the blue stars represent the mean collision times for the electron-impact ionization of argon and krypton, respectively. Since pump pulse intensity used in the case of argon (3.1×10^{14} W/cm²) is stronger than that for krypton (1.5×10^{14} W/cm²), the maximum kinetic energy of the electron considered for argon is correspondingly higher than that for krypton. As shown by the black triangles and the blue circles in Fig. 4(b), the mean collision time for the impact excitation by the fast electrons with a kinetic energy of >15 eV is around 5.5 ps for argon and around 3 ps for krypton, respectively. It indicates a significant population of the excited state by the EAC at these delays. Hence, a significant enhancement of the HH signal occurs around 5.5 ps for argon and around 3 ps for krypton, as shown in Fig. 4(a). The collision times for the electron-impact ionization of argon and krypton by the fast electrons are around 25 ps and around 20 ps, as shown by the black crosses and the blue stars, respectively. These values are very close to the delay where the harmonic enhancement starts to decay. This agreement indicates the electron-impact ionization starts to take an important role in the EAC process. The ionization due to the EAC not only decreases the population of the excited state but also increases the population of the ionized state, leading to the suppression of the HH emission. Consequently, the suppression region of the HHs is observed afterwards. After the electron-impact excitation and ionization, the fast electrons slow down to a very low kinetic energy. For very slow electrons, it is more likely to be captured by the ions than rescattered. Under this condition, the electron-impact recombination becomes the main result of the EAC process. Similarly, the HH signals start to revive after the delay of 100 ps for argon and 60 ps for krypton, as shown by the black triangles and blue circles in Fig. 4(a). After long enough time, gas plasma finally evolves into a neutral gas. Consequently, the HH signals are mostly emitted by the neutral atoms. The full revival of the HH signal is

observed around 400 ps for argon and around 200 ps for krypton, as shown in Fig. 4(a). Hence, the lifetimes of the gas plasma are 400 ps and 200 ps in the cases of argon and krypton, respectively.

From the above discussion, one can conclude that the three regions of the HH signal, i.e., the enhancement, the suppression, and the restoration regions, are associated with three EAC processes. In particular, after the generation of gas plasma by the pump pulse, atoms are initially excited by collisions between the remaining neutrals and the fast free electrons on the time scale of several picoseconds. Then a significant enhancement of HH signal shows up when a reasonable degree of the excitation is achieved, which lasts until the excited atoms are depleted by the further collision between the excited atoms and the free electrons on the time scale of a few tens of picoseconds. After the frequent collisions, the hot electrons slow down to a very low kinetic energy. Slow electrons are captured by the ions rather than being rescattered. Hence, the electron-impact recombination plays an important role in the EAC process, when the HHs start to revive. When the gas plasma dies out and the system becomes neutral, the HH signal reaches a full restoration. Accordingly, the lifetime of the generated gas plasma can be directly extracted from the HH spectroscopy. One can also note that the enhancement regions of the HH signal are different for argon and krypton. This may be attributed to their different collision cross sections. The larger collision cross section of krypton renders the excited states more easily disturbed by the free-electron impact. Correspondingly, the enhancement signal coming from its excited states dies out more rapidly.

It is worth noting that a very low gas pressure of about 20 Torr was used for both argon and krypton, and the probe intensity is not high enough to drive HH generation from the ionized state in our experiment. Under this low gas pressure, the effect of the neutral atom dispersion and the free electron dispersion is small when the ionization level is not too high. Consequently, the phase-matching condition does not change too much at different time delays. Hence, we neglect the role of propagating and phase-matching effects in our simple EAC model. Such a simple EAC model has already given a good qualitative explanation of the experimental data. However, a more comprehensive theory, considering the propagating and phase-matching effects, is still necessary for fully account for the underlying physics.

In conclusion, the EAC dynamics in argon and krypton gas plasma have been comprehensively investigated through the measurement of HH signals in a pump-probe scheme. The delay-dependent HH signals are featured by the first enhancement, the subsequent suppression, and the final restoration. We demonstrated that these features are well related to the EAC dynamics (the electron-impact excitation, the electron-impact ionization, and the electron-impact recombination). In short, the excited atoms are first generated by the collision between the neutrals with the early arriving electrons on the time scale of several picoseconds. Then they are depleted into ions by the further collisions with the later arriving electrons on the time scale of dozens of picoseconds. Finally, the neutrals are restored by the recombination of the ions with the latest arriving electrons with the slow velocity on the time scale of hundreds of picoseconds. This demonstrates that HH spectroscopy can be utilized to probe the EAC dynamics, and four important times during the evolution of gas plasma can be directly extracted from the HH

spectra. Our method to probe the EAC dynamics is also applicable to the study of other atoms or molecules.

Funding. National Natural Science Foundation of China (NSFC) (11474223, 11127901, 11227902, 11234004, 11404356, 11604248, 11774363, 61504082, 61521093, 61690223); ASTAR SERC Grant (1426500049, 1426500050); Global Research Laboratory Program (2009-00439); Max Planck POSTECH/KOREA Research Initiative Program (2016K1A4A4A01922028); Overseas Expertise Introduction Project for Discipline Innovation (111 Project, B12024).

[†]These authors contributed equally to this work.

REFERENCES

1. P. B. Corkum, *Phys. Rev. Lett.* **71**, 1994 (1993).
2. I. H. Hutchinson, *Plasma Phys. Controlled Fusion* **44**, 2603 (2002).
3. K. H. Kurniawan, M. O. Tjia, and K. Kagawa, *Appl. Spectrosc. Rev.* **49**, 323 (2014).
4. J. Dai, N. Karpowicz, and X.-C. Zhang, *Phys. Rev. Lett.* **103**, 023001 (2009).
5. S. Mityukovskiy, Y. Liu, P. Ding, A. Houard, A. Couairon, and A. Mysyrowicz, *Phys. Rev. Lett.* **114**, 063003 (2015).
6. B. L. Moiseiwitsch and S. J. Smith, *Rev. Mod. Phys.* **40**, 238 (1968).
7. S. Kaur, R. Srivastava, R. P. McEachran, and A. D. Stauffer, *J. Phys. B: At. Mol. Opt. Phys.* **31**, 4833 (1998).
8. L. Shi, W. Li, H. Zhou, L. Ding, and H. Zeng, *Opt. Lett.* **38**, 4 (2013).
9. M. R. H. Rvdge, *Rev. Mod. Phys.* **40**, 564 (1968).
10. M. Baertschy, T. N. Rescigno, and C. W. McCurdy, *Phys. Rev. A* **64**, 022709 (2001).
11. Z. Wu, G. Han, J. Yan, and J. Pang, *J. Phys. B: At. Mol. Opt. Phys.* **35**, 2305 (2002).
12. X. Yuan, P. Wei, C. Liu, Z. Zeng, Y. Zheng, J. Jiang, X. Ge, and R. Li, *Appl. Phys. Lett.* **107**, 041110 (2015).
13. Z. Zhai, Q. Zhu, J. Chen, Z. C. Yan, P. Fu, and B. Wang, *Phys. Rev. A* **83**, 043409 (2011).
14. P. M. Paul, T. O. Clatterbuck, C. Lyngå, P. Colosimo, L. F. DiMauro, P. Agostini, and K. C. Kulander, *Phys. Rev. Lett.* **94**, 113906 (2005).
15. I. A. Ivanov and A. S. Kheifets, *J. Phys. B: At. Mol. Opt. Phys.* **41**, 115603 (2008).
16. A. D. Shiner, B. E. Schmidt, C. Trallero-Herrero, H. J. Wörner, S. Patchkovskii, P. B. Corkum, J.-C. Kieffer, F. Légaré, and D. M. Villeneuve, *Nat. Phys.* **7**, 464 (2011).
17. H. J. Wörner, J. B. Bertrand, D. V. Kartashov, P. B. Corkum, and D. M. Villeneuve, *Nature* **466**, 604 (2010).
18. O. Smirnova, Y. Mairesse, S. Patchkovskii, N. Dudovich, D. Villeneuve, P. Corkum, and M. Yu. Ivanov, *Nature* **460**, 972 (2009).
19. F. Lépine, M. Y. Ivanov, and M. J. J. Vrakking, *Nat. Photonics* **8**, 195 (2014).
20. L. He, Q. Zhang, P. Lan, W. Cao, X. Zhu, C. Zhai, F. Wang, W. Shi, M. Li, X. Bian, P. Lu, and A. D. Bandrauk, *Nat. Commun.* **9**, 1108 (2018).
21. T. T. Luu, M. Garg, S. Yu. Kruchinin, A. Moulet, M. Th. Hassan, and E. Goulielmakis, *Nature* **521**, 498 (2015).
22. P. Antoine, A. L'huillier, and M. Lewenstein, *Phys. Rev. A* **53**, 1725 (1996).
23. M. V. Ammosov, N. B. Delone, and V. P. Krainov, *Sov. Phys. JETP* **64**, 1191 (1986).
24. R. A. Ganeev, M. Suzuki, M. Baba, H. Kuroda, and T. Ozaki, *Opt. Lett.* **31**, 1699 (2006).
25. D. B. Milošević, *J. Opt. Soc. Am. B* **23**, 308 (2006).
26. D. B. Milošević, *J. Phys. B: At. Mol. Opt. Phys.* **40**, 3367 (2007).
27. D. B. Milošević, *Phys. Rev. A* **81**, 023802 (2010).
28. R. W. Wagenaar and F. J. Heer, *J. Phys. B: At. Mol. Phys.* **18**, 2021 (1985).
29. K. P. Subramanian and V. Kumar, *J. Phys. B: At. Mol. Phys.* **20**, 5505 (1987).
30. Scattering cross sections, Biagi-v7.1, <http://nl.lxcat.net/home/>.